UWL REPOSITORY

repository.uwl.ac.uk

Mapping the spatial variation of soil moisture at the large scale using GPR for pavement applications

This is the Accepted Version of the final output.

UWL repository link: https://repository.uwl.ac.uk/id/eprint/2193/

Alternative formats: If you require this document in an alternative format, please contact: open.research@uwl.ac.uk

Mapping the spatial variation of soil moisture at the large scale using GPR for pavement applications

Andrea Benedetto[1,*], Fabio Tosti[1], Bianca Ortuani[2], Mauro Giudici[3,4], Mauro Mele[5]

[1] Department of Engineering, Roma Tre University, Via Vito Volterra 62, 00146, Rome, Italy

[2] Institute of Agricultural Hydraulics, Università degli Studi di Milano, Via Celoria 2, 20133, Milan, Italy

[3] Earth Sciences Department "A. Desio" & CINFAI, Università degli Studi di Milano, Via Cicognara 7, 20129 Milan, Italy

[4] CNR-IDPA, Via Mario Bianco 9, 20131, Milan, Italy

[5] Earth Sciences Department "A. Desio", Università degli Studi di Milano, Via Mangiagalli 33, 20133 Milan, Italy

* Corresponding author: mail: andrea.benedetto@uniroma3.it; tel: +39 0657333543

Abstract

The characterization of shallow soil moisture spatial variability at the large scale is a crucial issue in many researches and fields of application ranging from agriculture, geology, civil and environmental engineering. In this framework, this work contributes to the research in the area of pavement engineering for preventing damages and planning effective management. High spatial variations of subsurface water content can lead to unexpected damages of the load-bearing layers; thus, both safety and operability of roads become lower, thereby affecting an increase of expected accidents.

A pulse ground-penetrating radar (GPR) system with ground-coupled antennas, 600 MHz and 1600 MHz center frequencies of investigation, was used to collect data in a 16m $\times$ 16m study site in the Po valley area, in northern Italy. Two GPR techniques were employed to non-destructively retrieve the subsurface moisture spatial profile. The first technique is based on the evaluation of the dielectric permittivity from the signal amplitudes attenuation. Therefore, dielectrics were converted into moisture values using soil-specific coefficients from Topp's relationship. GPR-derived values of soil moisture were then compared with measurements from eight capacitance probes. The second technique is based on the Rayleigh scattering of the signal from the Fresnel theory, wherein the shifts of the peaks of frequency spectra are assumed to be comprehensive indicators for characterizing the spatial variability of moisture. Both GPR methods have shown great promises for mapping the spatial variability of soil moisture at the large scale.

List of keywords

ground-penetrating radar; soil moisture; road pavement; Rayleigh scattering; capacitance probe

INTRODUCTION

Subsurface spatial distribution of soil moisture is a primary factor in many researches and fields of application ranging from agriculture, geology, civil and environmental engineering (Giudici 2004; Romano and Giudici 2007; Baroni *et al.* 2010). It is well known that small-scale variability in soil hydraulic properties at the centimeter scale affects the spatial variability of moisture content (Ritsema and Dekker 1998), and large-scale variability is of great concern at the kilometer scale (Jackson and Le Vine 1996).

In that respect, different techniques for soil moisture sensing with different temporal and spatial scales capabilities are increasingly developing (Robinson *et al.* 2008a,b; Vereecken *et al.* 2008). In particular, moisture in soils is widely evaluated by using high-frequency electromagnetic (EM) techniques, due to the large influence brought by the permittivity of water on the relative dielectric permittivity of soils (Topp *et al.* 1980). Results and potentialities of remote sensing in large-scale areas ($> 100 \text{ m}^2$) investigations can be found in Wagner et al. (2007). Nevertheless, the huge footprint of such instruments is linked to a low resolution of radar sensors (~10 m) even for high-resolution active radar sensors. Small measurement depths and the inability to detect moisture content in a densely vegetated environment are additional drawbacks to be taken into account for remote sensing (Ulaby *et al.* 1996). Conversely, point information can be obtained at much finer scales (area $< 0.01 \text{ m}^2$) using different techniques, such as time domain reflectometry (TDR) (Greco and Guida 2008), and capacitance probes (Giraldi and Iannelli 2009), or volumetric sampling. These methods enable to collect a large amount of data at a tiny temporal resolution in a fine-scale domain (from ~10^{-2} m to 10^{-1} m), but are time-consuming for an effective mapping of larger areas. In addition, such techniques are intrusive to the soil structure, frequently resulting in inaccurate volumetric water content measurements (Lunt *et al.* 2005).

In line with this general framework, a need for soil water content measurement techniques providing numerous, time-efficient, and detailed values at the intermediate-scale domain (from ~10^{-1} m to 1 m) is therefore observed. Over the last years ground-penetrating radar (GPR) has proven to be one of the most reliable geophysical inspection tools that can be employed in a wide

range of applications, such as mapping shallow subsurface soil properties. Basically, GPR allows to detect the main physical properties of subsurface through the transmission/reception of electromagnetic waves in a given frequency band (Daniels 2004; van der Kruk and Slob 2004). Recent GPR advances are thoroughly described by Slob *et al.* (2010). In soil sciences, GPR is used for estimating subsurface moisture content during irrigation and drainage cycles (Galagedara *et al.* 2005). Furthermore, it is employed in Earth sciences for monitoring soils, bedrock, groundwater, and ice (Le Gall *et al.* 2008; Evans 1966; Mele *et al.* 2012), and for natural hazards management and prevention purposes with the goal to ensure the geotechnical stability of important lifelines, such as road and rail infrastructures (Benedetto *et al.* 2011; Benedetto *et al.* 2012a; Hugenschmidt 2000).

In that respect, the main GPR-based applications in pavement engineering include the evaluation of layer thicknesses (Al-Qadi and Lahouar 2004), the detection of voids and cracks underneath pavements (Lau *et al.* 1992; Benedetto 2013), asphalt stripping monitoring (Scullion *et al.* 1994), the detection of reinforcing bars (Hugenschmidt and Loser 2008; Huston *et al.* 1999) and delamination of concrete (Dérobert *et al.* 2009; Kalogeropoulos *et al.* 2013), the location of utilities (Ayala-Cabrera *et al.* 2011), and bridges inspections (Benedetto *et al.* 2012b). It is also worth noting the great capability of such instrument to be used together with other non-destructive techniques, such as the light falling weight deflectometer (Benedetto *et al.* 2014), for collecting geometrical, physical, and mechanical properties of subsurface. Recent researches have been devoted toward the GPR-based evaluation of clay content in soils causing structural damages in pavements (Patriarca *et al.* 2013; Tosti and Benedetto 2012; Tosti *et al.* 2013), and new challenges are currently addressed on the possibility to infer the mechanical properties of load-bearing layers from their electrical characteristics (Benedetto and Tosti 2013a; , Tosti *et al.* 2014b). With regard to the monitoring of subsurface volumetric water content, research focused on the entire pavement structure (Al-Qadi *et al.* 2004) as well as on typical subgrade soils (Grote *et al.* 2003, Benedetto 2010, Benedetto *et al.* 2013, Lambot *et al.* 2004a, Tosti 2013) have been developed. More in general, a comprehensive review of GPR applications for soil moisture sensing can be found in

Huisman *et al.* (2003). In this regard, many studies have been carried out using GPR ground-wave techniques (Benedetto and Pensa 2007; Grote 2003; Hubbard *et al.* 2003; Huisman *et al.* 2002). Steelman and Endres (2011) developed another theoretical method that deals with the use of volumetric dielectric mixing formulae by correlating the dielectric permittivity of each soil constituent to its volume fraction. Conversely, amongst the various petrophysical empirical relationships available, Topp *et al.* (1980) soil-specific correlations are the most commonly used for converting the values of complex permittivity of unsaturated soils into moisture.

Over the last few years research in subsurface soil moisture content is increasingly being focused on the use of efficient and self-consistent techniques, capable to avoid or minimize the use of destructive core sampling, for calibration steps, thus optimizing the management of economic resources. In this regard, Benedetto (2010) used a Rayleigh scattering-based method for directly evaluating the volumetric water content in soils, without the need of a petrophysical relationship and calibration of the system. In addition, Lambot *et al.* (2004a) evaluated the dielectric properties of unsaturated soils under controlled moisture conditions by correlating the imaginary part of the dielectric permittivity to the frequency of the surveying electromagnetic waves.

Concerning the development of more efficient GPR configurations for large-scale inspections, many efforts have been devoted to improve the potentialities of off-ground radar systems (Redman *et al.* 2002; Saarenketo and Scullion 2000, Tosti *et al.* 2014a). In that respect, high effective techniques based on inverse modeling of mono-static radar systems have been developed and are currently being improved (Lambot *et al.* 2004b; Lambot *et al.* 2006; Minet *et al.* 2011).

METHODOLOGY AND OBJECTIVES

The main goal of the present paper is to provide a contribution to the research for preventing structural damages caused by the interaction between subsurface moisture content and load-bearing soils under the pavement structure, since the evaluation of the spatial distribution of soil moisture is a key issue in this research field.

In particular, the ability of GPR to evaluate the spatial variation of shallow soil moisture at the large scale has been analyzed. A pulse GPR system with ground-coupled antennas, 600 MHz and 1600 MHz center frequencies of investigation, was used over a 16m × 16m study site to map the soil moisture with a relatively high spatial resolution. The reliability of GPR data was evaluated by two independent methods for the estimate of soil water content. First, soil moisture values were derived from the evaluation of the relative dielectric permittivity of soils assessed by the attenuation of signal amplitudes (Maser and Scullion 1990), as a result of reflections from the subsurface. The Topp petrophysical empirical relationship (Topp *et al.* 1980) was used for converting the dielectrics into moisture. Therefore, such moisture values were locally compared with the volumetric water contents from eight capacitance probes evenly placed over the entire surveyed area. From now on, this first approach will be referred to as the "reflectivity method". The second method, which will be referred to as the "Rayleigh scattering method", uses a Rayleigh scattering-based approach for obtaining the peaks of the frequency spectra from the signals collected in the time domain (Benedetto 2010), so that a proxy of the subsurface moisture spatial field can be generated. Finally, the two obtained maps were compared by normalizing the values assumed by the respective moisture indicators.

THEORETICAL BACKGROUND

The "reflectivity method"

<u>Relative dielectric permittivity evaluation by surface reflection method</u>

It is well known that the electromagnetic characteristics of materials affect the amplitude of the received GPR signals. In particular, the relative dielectric permittivity of soil is widely influenced by the amount of water in soil pore spaces, due to much lower values of the solid matrix permittivity compared to that of water. Then, the variations of signal amplitudes are very sensitive to moisture content, and the higher the differences between the values of dielectric permittivity of adjacent interfaces, the greater will be the reflected amplitudes.

According to the aforementioned principle, the relative dielectric permittivity of the unsaturated

soil can be estimated by considering the maximum amplitude in absolute value of the first

reflected signal from the ground surface, related to the maximum amplitude in absolute value of

the first reflected signal from a copper sheet as follows:

$$\varepsilon_r = \left[\frac{1+A_0 \big/ A_{PEC}}{1-A_0 \big/ A_{PEC}} \right]^2 \qquad (1)$$

where ε_r is the relative dielectric permittivity of the shallow soil laying above the reflecting

surface, A_0 [V] and A_1 [V] are the amplitude values of reflections from, respectively, the soil

surface and a perfect electric conductor (PEC) situated at the same distance as the soil. The main

advantage of this approach is that it could be used for rapidly mapping shallow subsurface

dielectrics performing measurements with a fixed, single-offset GPR configuration when shallow

permittivity contrast interfaces are present. It is worth noting that the soil electric conductivity σ

and magnetic permeability μ are neglected in equation (1). Permittivity estimation through this

method is traditionally carried out using off-ground radar systems in far-field conditions, although

some recent researches based on data collected from air-coupled radars have also dealt with the

assessment of electromagnetic constitutive parameters in near-field conditions using data from

ground-coupled radar systems (Mertens et al. 2014; Mourmeaux et al. 2014). Another widely used

method for shallow soil permittivity estimation with ground-coupled radar systems is the direct

ground wave method, wherein by measuring the direct ground wave travel time t_{gw} [s] from the

transmitter to the receiver, it is possible to calculate the ground wave velocity v [m/s] by L/t_{gw},

where L [m] is the separation between the transmitting and receiving antenna. The relative

dielectric permittivity of the soil ε_r can be then evaluated by the expression $\varepsilon_r=(c/v)^2$, where c is

the speed of light in vacuum. Notwithstanding the potential of the direct wave method, some

drawbacks were identified by Huisman *et al.* (2003) including *i)* difficulties in separating the

ground wave from refracted and reflected waves, *ii)* difficulties in determining the proper antenna

separation in field with varying soil water content, *iii)* high attenuation of the ground wave causing constraints in the maximum antenna separation.

_θ_ values from the site-specific Topp petrophysical relationship

Once the relative dielectric permittivity ε_r is estimated using equation (1), the shallow volumetric water content θ [m^3·m^{-3}] can be computed by inverting the following soil-specific Topp petrophysical relationship (Topp *et al.* 1980):

$$\varepsilon_r = 1.74 - 0.34 \cdot \theta + 135 \cdot \theta^2 - 55.3 \cdot \theta^3 \tag{2}$$

It is worth mentioning that according to Topp's research, such expression is characterized by one of the lower errors of estimate among the various types of soil analyzed by the authors, being the error on the dielectric permittivity equal to 0.38, to which an error of 1.8×10^{-2} for the estimates of θ is associated.

The "Rayleigh scattering method"

This approach is focused on the Rayleigh scattering of the signal on the basis of the Fresnel theory (Benedetto 2010). It is well known that scattering is generated by singularities or non-homogeneities (e.g., water droplets and soil particles) in electromagnetic impedance, and the process occurs when their dimensions are much smaller than the wavelength of the EM wave. From an analytical point of view, the ratio $x = 2\pi r/\lambda$ defines the size of a scattering particle, where r is the radius of the particle, and λ is the wavelength of the signal. Rayleigh scattering occurs in the small size parameter regime $x \ll 1$. On the contrary, Mie (1908) theory deals with scattering from large spherical particles for an arbitrary size parameter x; in particular, for small values of x the Mie theory reduces to the Rayleigh approximation.

By considering several assumptions on the three-phase porous medium properties, and simplifications of the physics, it is possible to define the following formulation (Benedetto 2010):

$$I(\phi, f) = I_0(f)\frac{1+\cos^2\theta_s}{2R^2}\left[\frac{2\pi v}{c_0}\sqrt{\mu_r\left(\varepsilon_\infty + \frac{\Delta\varepsilon}{1+f^2\tau^2}\right)}\right]^4\left[\frac{\mu_r\left(\varepsilon_\infty + \frac{\Delta\varepsilon}{1+f^2\tau^2}\right)-1}{\mu_r\left(\varepsilon_\infty + \frac{\Delta\varepsilon}{1+f^2\tau^2}\right)+2}\right]^2\left(\frac{d}{2}\right)^6 \tag{3}$$

where $I(\phi, f)$ is the intensity of the EM wave scattered by a single small particle, R is the distance between the observer and the particle, θ_s is the angle of scattering, f is the frequency of the EM signal, c_0 is the speed of light in vacuum, μ_r is the magnetic permeability, ε_∞ is the dielectric constant of the full-polarized medium at an infinite frequency EM field, $\Delta\varepsilon = \varepsilon_{static} - \varepsilon_\infty$ is the difference between the values of permittivity of a steady and an infinite frequency EM field, τ is the relaxation time, and d is the diameter of the particle. In this approach, the processing of the signal is carried out in the frequency domain. Outcomes from past researches developed on various types of unsaturated porous media, have shown that scattering produces a non-linear modulation of the electromagnetic signal, as a function of the moisture content (Benedetto and Tosti 2013b). According to equation (3), the various frequency components of the frequency spectra are differently scattered, depending on both soil texture and moisture content. Therefore, by comparing the frequency spectra of the signals collected under different moisture conditions, it is possible to retrieve information on the near-surface moisture content of each investigated soil. In particular, the peak of frequency was observed by Benedetto (2010) to be a comprehensive indicator, negatively related to moisture. In this regard it has to be noted that, since scattering is caused by water presence in the medium, more scattering events are expected in the form of frequency peak shifting, as the moisture content increases (Benedetto 2010). Several correlations were provided between the shift of the peak and moisture content for different types of soil under controlled laboratory conditions. The general expression for predicting volumetric moisture content θ [%] is defined as (Benedetto 2010):

$$\theta = (A - f_P)/B \tag{4}$$

where A and B are regression parameters calibrated by experiments on different soil samples, and f_P [Hz $\times$ 10^8] is the value of the peak of frequency. It is worth mentioning that, from a theoretical

point of view, being f_P the value of frequency for which the value of $I(\phi, f)$ is maximum, it can be determined by letting to 0 the first derivative of equation (3), calculated as a function of f.

In the present paper, the peaks of the frequency spectra obtained over the entire surveyed area have been mapped to generate a proxy of the near-surface moisture spatial field.

EXPERIMENTAL FRAMEWORK

Tools and equipment

A GPR with two ground-coupled antennas, 600 MHz and 1600 MHz center frequencies of investigation (RIS 99-MF Multi Frequency Array Radar-System manufactured by IDS S.p.A., Italy) was used for the surveys (Figure 1a). Measurements were carried out using 4 channels, 2 mono-static and 2 bi-static. Data were acquired in the time domain, in a 40 ns time window with a time step $dt = 7.8125 \times 10^{-2}$ ns. Horizontal sampling resolution amounted to 2.4×10^{-2} m. According to the main goal of this study, only the 600 MHz mono-static channel was processed. The 1600 MHz mono-static signal and the two bi-static ones were used for cross-checking.

Capacitance probes WaterScout SM100 manufactured by Spectrum Technologies Inc. (Figure 1b) were evenly placed over the entire surveyed area, collecting data at depths of 0.15 m and 0.45 m below the ground surface to provide point information on subsurface moisture content. According to the depth domain of the shallow soil dielectric parameters assessed by equation (1), only the data related to 0.15 m deep were used for comparison.

FIGURE 1 a) Ground-coupled antenna pulse radar system, 600 MHz and 1600 MHz center frequencies of investigation, manufactured by IDS S.p.A. b) Capacitance probe WaterScout SM100 manufactured by Spectrum Technologies Inc.

Capacitance probes were calibrated by gathering undisturbed soil samples of the same volume of the support explored by the probe as close to the sampling points. The gravimetric water content w [g·g^{-1}] was measured in laboratory environment and transformed in volumetric water content θ,

so that the site-specific calibration curve was determined. A relatively good agreement was found between the direct (w) and indirect (θ) soil moisture measurements as the mean absolute relative error and the coefficient of determination were 13% and 0.89, respectively (Figure 2). A detailed description of moisture statistics on the entire survey campaign can be found in Ortuani *et al.* 2013.

FIGURE 2. Site-specific calibration curve for capacitance probes relating gravimetric (w) and volumetric water content (θ).

Study site, weather conditions, and soil properties

The test site is situated in the Po valley area, in northern Italy, near the town of Landriano (9° 16' 12" E, 45° 19' 23" N), as shown in Figure 3.

The average elevation is approximately 88 m a.s.l., with an almost flat ground along the entire surveyed field. The area is characterized by a semi-humid climate with mean annual precipitation and temperature of 880 mm and 12 °C, respectively. Soil type is a pretty uniform, bare, sandy loam characterized by a low surface roughness, with an average amplitude of 0.05 m, whose effects on the electromagnetic parameters herein analyzed have been verified to be negligible in near-field conditions [Mourmeaux *et al.* 2014]. Table 1 lists the grain size distribution of a representative soil sample collected within the test site area.

TABLE 1. Grain size distribution of a soil sample collected within the test site area.

According to the requirements for the applicability of the "Rayleigh scattering" method, by reasonably considering the water within the investigated three-phase porous medium as mostly fixed to grain particles by means of capillary action, it is possible to take into account the grain size of 0.075×10^{-3} m as a reference average dimension for the whole soil particles, on the basis of the highest percentage of material retained at sieve $P_{0.075}$ (i.e., Table 1). Therefore, by using a

600 MHz center frequency of investigation and with regard to the quarter of wavelength criteria, it is possible to verify that Rayleigh scattering occurs in the small size parameter regime $x \ll 1$. Accordingly, the same reference particle size of 0.075×10^{-3} m has been considered as the value of d into equation (3).

The GPR campaign took place at the beginning of autumn, on October 2nd, 2012, in moderately wet conditions. According to the nearest rain gauge station, low rainfall was recorded during the previous seven days (< 8 mm/day, on the average), with a medium level of evaporation due to the medium-high temperatures in that period (17 °C, on the average).

A 16m × 16m field was mapped with the GPR, following a 17 × 17 lines square grid pattern with a spacing of 1 m between the acquisition tracks. The GPR was dragged with a driving speed of about 3 km/h (almost 1 m/s), for a total collection of 21300 measured points.

Furthermore, eight capacitance probes were uniformly distributed over the surveyed area for collecting moisture at 0.15 m depth below the ground surface in order to compare the shallow soil moisture assessed through the "reflectivity method".

FIGURE 3. Study site for the GPR acquisition carried out over a 16-m × 16-m area, 1-m spacing between the tracks (17 × 17 lines square grid pattern).

RESULTS AND DISCUSSION

Punctual comparison of moisture data

A comparison between the moisture data retrieved by GPR (θ_{GPR}) using the "reflectivity" method, and those collected by eight capacitance probes (θ_{probe}) is shown in Figure 4. An overall good agreement can be observed between the GPR-derived and the probe-measured moisture, with the exception of stations 5 and 6, where the absolute residuals are equal to 0.048 m$^3 \cdot$m^{-3} and 0.067 m$^3 \cdot$m^{-3}, respectively. The average soil moisture from GPR at the eight probe stations amounts to 0.309 m$^3 \cdot$m^{-3} with a standard deviation of 0.0105 m$^3 \cdot$m^{-3}. The same statistics concerning soil moisture from capacitance probes are equal to 0.318 m^{3}m^{-3} and 0.0292 m^{3}m^{-3}, respectively.

FIGURE 4. Bar graphs representing GPR-derived (θ_{GPR}) and probe-measured (θ_{probe}) volumetric soil moisture contents at the eight probe sensing stations.

In order to better analyze the reliability of GPR-derived soil moisture, the relative incidence of residuals [%], defined by the ratio between the relative value of the residual and the corresponding moisture value from capacitance probe, is taken into account. In that respect, residuals are considered as the differences between probe-measured and GPR-derived moisture data (Figure 5). Overall, with the exception of the two aforementioned outliers, the variability of such incidences is observed within approximately the 8%. These mismatches can be reasonably due to the different support scale of the GPR-based technique, greater than the small-scale variability of soil moisture detected by capacitance probe.

FIGURE 5. Incidence of moisture residuals at the eight probe sensing stations.

Mapping of soil moisture spatial variability

Mapping of the normalized shallow subsurface dielectric water content from the "reflectivity" method

The field-average soil moisture inferred through the "reflectivity" method is equal to 0.351 $m^3 \cdot m^{-3}$, with a standard deviation of 0.030 $m^3 \cdot m^{-3}$. Therefore, a slightly higher variability of near-surface moisture content on the large scale is observed.

Concerning the spatial distribution of soil moisture, Figures 6a,b represent the interpolated normalized subsurface soil moisture θ_{NORM} from the GPR acquisition. The variogram model is linear, with slope of 1.513×10^{-4}, anisotropy ratio and angle of 2 and 87.72°, respectively, lag distance equal to 7.5 m, and nugget 0.0062. The field-average normalized moisture is equal to 0.762, with a standard deviation of 0.082. The coefficient of variation and the skewness measure 0.1078 and 0.3377, respectively. The highest values of moisture content are encountered in two

places, about 7 m from the northern edge of the surveyed area: one spot is located at about 5.5 m from the western edge of the grid pattern, and the second one at the eastern edge. On the contrary, the driest areas can be observed in the middle of the western edge and close to the south-eastern corner of the area. It is worth noting that given the flat landscape, the topography is not considered in the soil pattern.

FIGURE 6. a) Normalized shallow soil dielectric moisture (θ_{NORM}) map overlaid with iso-contour lines from the "reflectivity" method. b) Iso-contour lines of the normalized shallow soil dielectric moisture (θ_{NORM}) map from the "reflectivity" method.

Mapping of the normalized frequency peaks from the "Rayleigh scattering" method

Figures 7a,b show the map of the interpolated normalized frequency peaks f_{PNORM} extracted from the frequency spectra of the received signals using the "Rayleigh scattering" method. The variogram model is linear, with slope of 2.92×10^{-8}, anisotropy ratio and angle of 1000 and 134.8°, respectively, lag distance equal to 7.5 m, and nugget 0.0045. According to the correlations found by Benedetto (2010) between shifts of frequency peaks and subsurface moisture content variation, this map can be considered as a proxy of the near-surface moisture spatial field. The field-average normalized frequency peak is equal to 0.813, with a standard deviation of 0.068. Therefore, such method seems to account for a lower presence of wet spots over the entire area and a lower variability of moisture spatial distribution. The coefficient of variation and the skewness measure 0.0839 and 1.2787, respectively. In line with the aforementioned field-average values of normalized moisture and frequency peaks, the iso-contour lines in Figures 6a,b and 7a,b have been set to 0.8.

FIGURE 7. a) Normalized frequency peaks (f_{PNORM}) map overlaid with iso-contour lines from the "Rayleigh scattering" method. b) Iso-contour lines of the normalized frequency peaks (f_{PNORM}) from the "Rayleigh scattering" method.

Comparison between maps from the GPR-based methods

Figure 8 shows the comparison between the iso-contour lines of subsurface moisture obtained using the "reflectivity" and the "Rayleigh scattering" methods overlaid on the normalized near-surface soil moisture map. A good agreement with the theoretical expectations is demonstrated. In particular, a lowering of the peak of the frequency spectrum corresponds to an increase of dielectric permittivity, as the moisture content is expected to rise. On the contrary, from a decrease of the relative dielectric permittivity and an increase of the value of frequency peak, a lowering of moisture content is expected to be found. In this regard, a clear match can be found between the low normalized frequency peak values and the high normalized shallow subsurface dielectric moisture in the north-western part of the figure. Further matches can be observed in the middle of the western edge of the figure, as well as in the south-eastern corner. In such cases, high normalized frequency peak values indicate low normalized volumetric water content.

From the analysis of the aforementioned characteristics of the two variograms, both linearly modeled, it is outlined a greater spatial continuity provided by data from the "reflectivity" method. In addition, from the analysis of the dataset behind the two displayed maps of volumetric water contents for quantitatively estimating the goodness-of-fit statistic of the two relevant variograms, statistics concerning the median absolute deviation of the cross-validation residuals for the "reflectivity" and the "Rayleigh scattering" methods are equal to 0.0453 and 0.0298, respectively. In line with this, the "Rayleigh scattering" method provides moisture values less affected by statistical dispersion, along with a greater robustness statistics, as the deviations of outliers from the mean are less relevant. Statistics on standard deviation of the cross-validation residuals are equal to 0.0664 for the "reflectivity" method, and 0.0459 for the "Rayleigh scattering" method, thus indicating a better fitting for data from the "Rayleigh scattering" method.

FIGURE 8. - Normalized shallow soil dielectric moisture map overlaid with iso-contour lines from the "reflectivity" (solid black lines) and the "Rayleigh scattering" method (dashed red lines).

CONCLUSION

The paper proposes the application of two GPR-based approaches for monitoring soil moisture spatial field in pavement engineering applications, to prevent structural damaging. A GPR survey, including 21300 records over a 16m × 16m field, was carried out. Local comparisons were developed between the GPR-derived and the probe-measured moisture contents. Moreover, subsurface maps of both normalized shallow subsurface dielectric moisture and normalized frequency spectra peaks were processed.

Although some discrepancies were shown concerning local moisture comparisons, results demonstrated a greater effectiveness of the proposed GPR approaches for large-scale inspections, consistent with the dimension of the surveyed area. Overall, from the analysis of the best-fitting variograms characteristics for the dataset behind the moisture maps obtained from the "reflectivity" and the "Rayleigh scattering" methods, a greater spatial continuity provided by data from the "reflectivity" method has been outlined.

It is also worth noting that the application of the "reflectivity" method to data collected by means of a ground-coupled radar system, along the lines of the "surface reflection method" for the estimation of permittivity values of the type of soil investigated has proved to be suited for this purpose and capable to provide reliable values of volumetric water content at finer scales of investigation.

More insights about the reliability of results may be achieved by multiple repetitions of the GPR acquisitions which may be eased by the use of high-efficient GPR systems, such as off-ground radar systems.

References

Al-Qadi I.L. and Lahouar S. 2004. Use of GPR for thickness measurement and quality control of flexible pavements. Journal of the Association of Asphalt Paving Technologists 73, 501–528.

Al-Qadi I.L., Lahouar S., Loulizi A., Elseifi M.A. and Wilkes J.A. 2004. Effective approach to improve pavement drain-age layers. Journal of Transportation Engineering 130(5), 658–664. doi: 10.1061/(ASCE)0733-947X(2004)130:5(658).

Ayala-Cabrera D., Herrera M., Izquierdo J. and Pérez-García R. 2011. Location of buried plastic pipes using multi-agent support based on GPR images. Journal of Applied Geophysics 75(4), 679–686. doi: 10.1016/j.jappgeo.2011.09.024.

Baroni G., Facchi A., Gandolfi C., Ortuani B., Horeschi D. and van Dam J.C. 2010. Uncertainty in the determination of soil hydraulic parameters and its influence on the performance of two hydrological models of different complexity. Hydrology and Earth System Sciences 14, 251–270. doi: 10.5194/hess-14-251-2010.

Benedetto A. and Pensa S. Indirect diagnosis of pavement structural damages using surface GPR reflection techniques. Journal of Applied Geophysics 62(2), 107–123. doi: 10.1016/j.jappgeo.2006.09.001.

Benedetto A. 2010. Water content evaluation in unsaturated soil using GPR signal analysis in the frequency domain. Journal of Applied Geophysics 71, 26–35. doi: 10.1016/j.jappgeo.2010.03.001.

Benedetto A., Tosti F., Schettini G. and Twizere C. 2011. Evaluation of Geotechnical Stability of Road using GPR. In: *Proceedings of Sixth International Workshop on Advanced Ground Penetrating Radar*, Aachen, Germany, pp. 1–6. doi: 10.1109/IWAGPR.2011.5963858.

Benedetto A., Benedetto F. and Tosti F. 2012a. GPR applications for geotechnical stability of transportation infrastructures. Nondestructive Testing And Evaluation 27(3), 253–262. doi: 10589759.2012.694884.

Benedetto A., Manacorda G., Simi A. and Tosti F. 2012b. Novel perspectives in bridges inspection using GPR. Nondestructive Testing And Evaluation 27(3), 239–251.

Benedetto A. 2013. A three dimensional approach for tracking cracks in bridges using GPR. Journal of Applied Geophysics 97, 37–44. 10.1016/j.jappgeo.2012.12.010.

Benedetto A., Tosti F., Ortuani B., Giudici M. and Mele M. 2013. Soil Moisture Mapping using GPR for Pavement Applications. In: *Proceedings of the Seventh International Workshop on Advanced Ground Penetrating Radar*, Nantes, France, pp. 243-248. doi: 10.1109/IWAGPR.2013.6601550.

Benedetto A. and Tosti F. 2013a. Inferring bearing ratio of un-bound materials from dielectric properties using GPR: the case of Runaway Safety Areas. In: *Proceedings of the Airfield and Highway Pavement 2013 Conference*, Los Angeles, California, USA, pp. 1336-1347. doi: 10.1061/9780784413005.113.

Benedetto A., D'Amico F. and Tosti F. 2014. Improving safety of runway overrun through the correct numerical evaluation of rutting in Cleared and Graded Areas. Safety Science 62, 326–338. doi: 10.1016/j.ssci.2013.09.008.

Benedetto F. and Tosti F. 2013b. GPR spectral analysis for clay content evaluation by the frequency shift method. Journal of Applied Geophysics 97, 89–96. doi: 10.1016/j.jappgeo.2013.03.012.

Daniels D.J. 2004. Ground Penetrating Radar. The Institution of Electrical Engineers, London.

Dérobert X., Villain G., Cortas R. and Chazelas J.L. 2009. EM characterization of hydraulic concretes in the GPR frequency-band using a quadratic experimental design. In: Proceedings of the seventh international symposium NDT-CE, Nantes, France.

Evans S. 1966. Progress report on radio echo sounding. Polar Record 13(85), 413–420. doi: 10.1017/S0032247400057703.

Galagedara L.W., Parkin G.W., Redman J.D., von Bertoldi P. and Endres A.L. 2005. Field studies of the GPR ground wave method for estimating soil water content during irrigation and drainage. Journal of Hydrology 301, 182–197. doi: 10.1016/j.jhydrol.2004.06.031.

Giraldi D. and Iannelli R. 2009. Measurements of water content distribution in vertical subsurface flow constructed wetlands using a capacitance probe: benefits and limitations. Desalination 243, 182–194. doi: 10.1016/j.desal.2008.05.012.

Giudici M. 2004. Experimental and modeling studies of infiltration. In: *College on soil physics, ICTP lecture notes*. The Adbus Salaam International Centre for Theoretical Physics, pp. 191–198.

Greco R. and Guida A. 2008. Field measurements of topsoil moisture profiles by vertical TDR probes. Journal of Hydrology 348, 442–451. doi: 10.1016/j.jhydrol.2007.10.013.

Grote K., Hubbard S.S. and Rubin Y. 2003. Field-scale estimation of volumetric water content using GPR ground wave techniques. Water Resources Research 39(11), 1321. doi: 10.1029/2003WR002045.

Grote K., Anger C., Kelly B., Hubbard S. and Rubin Y. Characterization of soil water content variability and soil texture using GPR groundwave techniques. Journal of Environmental & Engineering Geophysics 15(3), 93–110. doi: 10.2113/JEEG15.3.93.

Hubbard S., Grote K. and Rubin Y. 2002. Estimation of nearsubsurface water content using high frequency GPR ground wave. The Leading Edge 21(6), 552–559.

Hugenschmidt J. 2000. Railway track inspection using GPR. Journal of Applied Geophysics 43(2), 147–155. doi: 10.1016/S0926-9851(99)00054-3.

Hugenschmidt J. and Loser R. 2008. Detection of chlorides and moisture in concrete structures with ground penetrating radar. Materials and Structures 41, 785–792. doi: 10.1617/s11527-007-9282-5.

Huisman J.A., Snepvangers J.J.J.C., Bouten W. and Heuvelink G.B.M. 2002. Mapping spatial variation in surface soil water content: comparison of ground penetrating radar and time domain reflectometry. Journal of Hydrology 269, 194–207. doi: 10.1016/S0022-1694(02)00239-1.

Huisman J.A., Hubbard S.S., Redman J.D. and Annan A.P. 2003. Measuring soil water content with ground penetrating radar: a review. Vadose Zone Journal 2, 476–491. doi: 10.2113/2.4.476.

Huston D.R., Hu J., Maser K., Weedon W. and Adam C. 1999. Ground penetrating radar for concrete bridge health monitoring applications. In: *Proceedings of SPIE* 3587, pp. 170-179. doi:10.1117/12.339922.

Jackson T.J. and Le Vine D.E. 1996. Mapping surface soil moisture using an aircraft-based passive microwave instrument: Algorithm and example. Journal of Hydrology 184, 85–99. doi: 10.1016/0022-1694(95)02969-9.

Kalogeropoulos A., van der Kruk J., Hugenschmidt J., Bikowski J. and Brühwiler E. 2013. Full-waveform GPR in-version to assess chloride gradients in concrete. NDT&E International 57, 74–84. doi: 10.1016/j.ndteint.2013.03.003.

Lambot S., Slob E.C., van den Bosch I., Stockbroeckx B. and Vanclooster M. 2004a. Modeling of ground-penetrating radar for accurate characterization of subsurface electric properties. IEEE Transactions on Geoscience and Remote Sensing 42, 2555–2568. doi: 10.1109/TGRS.2004.834800.

Lambot S., Slob E.C., van den Bosch I., Stockbroeckx B., Scheers B. and Vanclooster M. 2004b. Estimating soil dielectric properties from monostatic ground-penetrating radar signal inversion in the frequency domain. Water Resources Research 40(4), 1–12. W04 205. doi: 10.1029/2003WR002095.

Lambot S., Weihermüller L., Huisman J.A., Vereecken H., Vanclooster M. and Slob E.C. 2006. Analysis of air-launched ground-penetrating radar techniques to measure the soil surface water content. Water Resources Research 42(11), W11403. doi: 10.1029/2006WR005097.

Lau C.L., Scullion T. and Chan P. 1992. Modeling of ground-penetrating radar wave propagation in pavement systems. Transportation Research Record 1355, 99–107.

Le Gall A., Ciarletti V., Berthelier J.-J., Reineix A., Guiffaut C., Ney R., Dolon F. and Bonaime S. 2008. An imaging HF GPR using stationary antennas: experimental validation over the Antarctic ice sheet. Geoscience and Remote Sensing. IEEE Transactions on 46(12), 3975–3986. doi: 10.1109/TGRS.2008.2000718.

Lunt I.A., Hubbard S. and Rubin Y. 2005. Soil moisture content estimation using ground-penetrating radar reflection data. Journal of Hydrology 307, 254–269. doi: 10.1016/j.jhydrol.2004.10.014.

Maser and K.R. and Scullion T. 1990. *Automated detection of pavement layer thicknesses and subsurface moisture using ground penetrating radar*. Infrasense, Inc.

Mele M., Bersezio R. and Giudici M. 2012. Hydrogeophysical imaging of alluvial aquifers: electrostratigraphic units in the quaternary Po alluvial plain (Italy). International Journal of Earth Sciences 101(7), 2005-2025. doi: 10.1007/s00531-012-0754-7.

Mertens L., Tran A.P. and Lambot S. 2014. Determination of the stability of a pulse GPR system and quantification of the drift effect on soil material characterization by full-wave inversion. In: *Proceedings of the 15th International Conference on Ground Penetrating Radar GPR 2014*, Bruxelles, Belgium. pp. 498-502.

Mie G. 1908. Beiträge zur Optik trüber Medien, speziell kolloidaler Metallösungen. Annalen der Physik 330, 377. doi: 10.1002/andp.19083300302.

Minet J, Wahyudi A., Bogaert P., Vanclooster M. and Lambot S. 2011. Mapping shallow soil moisture profiles at the field scale using full-waveform inversion of ground penetrating radar data. Geoderma 161, 225–237. doi: 10.1016/j.geoderma.2010.12.023.

Mourmeaux M., Tran A.P. and Lambot S. 2014. Soil permittivity and conductivity characterization by full-wave inversion of near-field GPR data. In: *Proceedings of the 15th International Conference on Ground Penetrating Radar GPR 2014*, Bruxelles, Belgium. pp. 516-521.

Ortuani B., Benedetto A., Giudici M., Mele M., and Tosti F. 2013. A non-Invasive approach to monitor variability of soil water content with electromagnetic methods. In: *Proceedings of the International Conference on Four Decades of Progress in Monitoring and Modeling of Processes in the Soil-Plant-Atmosphere System: Applications and Challenges*, Naples, Italy. Procedia Environmental Sciences, 19, pp. 446-455. doi: 0.1016/j.proenv.2013.06.051.

Patriarca C., Tosti F., Velds C., Benedetto A., Lambot S. and Slob E.C. 2013. Frequency dependent electric properties of homogeneous multi-phase lossy media in the ground-penetrating radar frequency range. Journal of Applied Geophysics 97, 81–88. doi: 10.1016/j.jappgeo.2013.05.003.

Redman J., Davis J., Galagedara L. and Parkin G. 2002. Field studies of GPR air launched surface reflectivity measurements of soil water content. In: *Proceedings of the Ninth International Conference on Ground Penetrating Radar*, Santa Barbara, California, USA. S. Koppenjan and K. Lee, Eds. 4758, pp. 156-161.

Ritsema C.J. and Dekker L.W. 1998. Three-dimensional patterns of moisture, water repellency, bromide and pH in a sandy soil. Journal of Contaminant Hydrology 31, 295–313. doi: 10.1016/S0169-7722(97)00067-3.

Robinson D.A., Binley A., Crook N., Day-Lewis F.D., Ferre T.P.A., Grauch V.J.S., Knight R., Knoll M., Lakshmi V., Miller R., Nyquist J., Pellerin L., Singha K. and Slater L. 2008a. Advancing process-based watershed hydrological research using near-surface geophysics: a vision for, and review of, electrical and magnetic geophysical methods. Hydrological Processes 22 (18), 3604–3635. doi: 10.1002/hyp.6963.

Robinson D.A., Campbell C.S., Hopmans J.W., Hornbuckle B.K., Jones S.B., Knight R., Ogden F., Selker J. and Wendroth O. 2008b. Soil moisture measurement for ecological and hydrological watershed-scale observatories: a review. Vadose Zone Journal 7(1), 58–389. doi: 10.2136/vzj2007.0143.

Romano E. and Giudici M. 2007. Experimental and modeling study of the soil-atmosphere interaction and unsaturated water flow to estimate the recharge of a phreatic aquifer. Journal of Hydrologic Engineering 12, 573–584. doi: 10.1061/(ASCE)1084-0699(2007)12:6(573).

Saarenketo T. and Scullion T. 2000. Road evaluation with ground penetrating radar. Journal of Applied Geophysics 43(2), 119–138. doi: 10.1016/S0926-9851(99)00052-X.

Scullion T., Lau C.L. and Chen Y. 1994. Pavement evaluations using ground penetrating radar. International Conference on Ground Penetrating Radar. In: *Proceedings of the Fifth International Conference on Ground Penetrating Radar*, Kitchener, Ontario, Canada, pp. 449-463.

Slob E.C., Sato M. and Olhoeft G. 2010. Surface and borehole ground-penetrating-radar developments. Geophysics 75(5), A103-A120. doi: 10.1190/1.3480619.

Steelman C.M. and Endres A.L. 2011. Comparison of petrophysical relationships for soil moisture estimation using gpr ground waves. Vadose Zone Journal 10, 270–285. doi: 10.2136/vzj2010.0040.

Topp G.C., Davis J.L. and Annan A.P. 1980. Electromagnetic determination of soil water content: measurements in coaxial transmission lines. Water Resources Research 16, 574–582. doi: 10.1029/WR016i003p00574.

Tosti F. and Benedetto A. 2012. Pavement pumping prediction using ground penetrating radar. In: *Proceedings of the Fifth International Congress SIIV on Sustainability of Road Infrastructures*, Rome, Italy, 53, pp. 1044-1053. doi: 10.1016/j.sbspro.2012.09.954.

Tosti F. 2013. Determination, by using GPR, of the volumetric water content in structures, substructures, foundations and soil. State of the art and open issues. Civil Engineering Applications of Ground Penetrating Radar. In: Proceedings of the First COST Action General Meeting TU1208, Rome, Italy. pp. 99-105.

Tosti F., Patriarca C., Slob E.C., Benedetto A. and Lambot S. 2013. Clay content evaluation in soils through GPR signal processing. Journal of Applied Geophysics 97, 69–80. doi: 10.1016/j.jappgeo.2013.04.006.

Tosti F., Benedetto A., and Calvi A. 2014a. Efficient air-launched ground-penetrating radar inspections in a large-scale road network. In Proceedings of the 3rd International Conference on Transportation Infrastructure, Pisa, Italy, Apr. 2014, pp. 703–709.

Tosti F., Adabi S., Pajewski L., Schettini G. and Benedetto A, 2014b. Large-Scale Analysis of Dielectric and Mechanical Properties of Pavement using GPR and LFWD. In: *Proceedings of the*

15th International Conference on Ground Penetrating Radar GPR 2014, Bruxelles, Belgium. pp. 898-903.

Ulaby F.T., Dubois P.C. and van Zyl J. 1996. Radar mapping of surface soil moisture. Journal of Hydrology 184, 57–84. doi: 10.1016/0022-1694(95)02968-0.

van der Kruk J. and Slob E.C. 2004. Reduction of reflections from above surface objects in GPR data. Journal of Applied Geophysics 55, 271–278. doi: 10.1016/j.jappgeo.2004.02.002.

Vereecken H., Huisman J.A., Bogena H., Vanderborght J., Vrugt J.A. and Hopmans, J.W. 2008. On the value of soil moisture measurements in vadose zone hydrology: a review. Water Resources Research 44(4), W00D06. doi: 10.1029/2008WR006829.

Wagner W., Blöschl G., Pampaloni P., Calvet J.C., Bizzarri B., Wigneron J.P. and Kerr Y. 2007. Operational readiness of microwave remote sensing of soil moisture for hydrologic applications. Nordic Hydrology 38(1), 1–20. doi: 10.2166/nh.2007.029.

List of captions

FIGURE 1 a) Ground-coupled antenna pulse radar system, 600 MHz and 1600 MHz center frequencies of investigation, manufactured by IDS S.p.A. b) Capacitance probe WaterScout SM100 manufactured by Spectrum Technologies Inc.

FIGURE 2. Site-specific calibration curve for capacitance probes relating gravimetric (w) and volumetric water content (θ).

TABLE 1. Grain size distribution of a soil sample collected within the test site area.

FIGURE 3. Study site for the GPR acquisition carried out over a 16-m $\times$ 16-m area, 1-m spacing between the tracks (17 $\times$ 17 lines square grid pattern).

FIGURE 4. Bar graphs representing GPR-derived (θ_{GPR}) and probe-measured (θ_{probe}) volumetric soil moisture contents at the eight probe sensing stations.

FIGURE 5. Incidence of moisture residuals at the eight probe sensing stations.

FIGURE 6. a) Normalized shallow soil dielectric moisture (θ_{NORM}) map overlaid with iso-contour lines from the "reflectivity" method. b) Iso-contour lines of the normalized shallow soil dielectric moisture (θ_{NORM}) map from the "reflectivity" method.

FIGURE 7. a) Normalized frequency peaks (f_{PNORM}) map overlaid with iso-contour lines from the "Rayleigh scattering" method. b) Iso-contour lines of the normalized frequency peaks (f_{PNORM}) from the "Rayleigh scattering" method.

FIGURE 8. a) Normalized shallow soil dielectric moisture map overlaid with iso-contour lines from the "reflectivity" (solid black lines) and the "Rayleigh scattering" method (dashed red lines).

Figures

FIGURE 1 a) Ground-coupled antenna pulse radar system, 600 MHz and 1600 MHz center frequencies of investigatio, manufactured by IDS S.p.A.

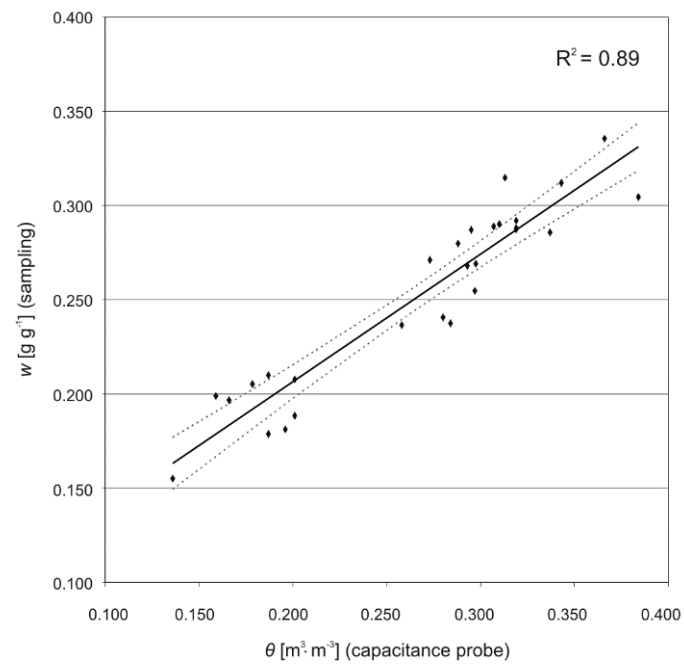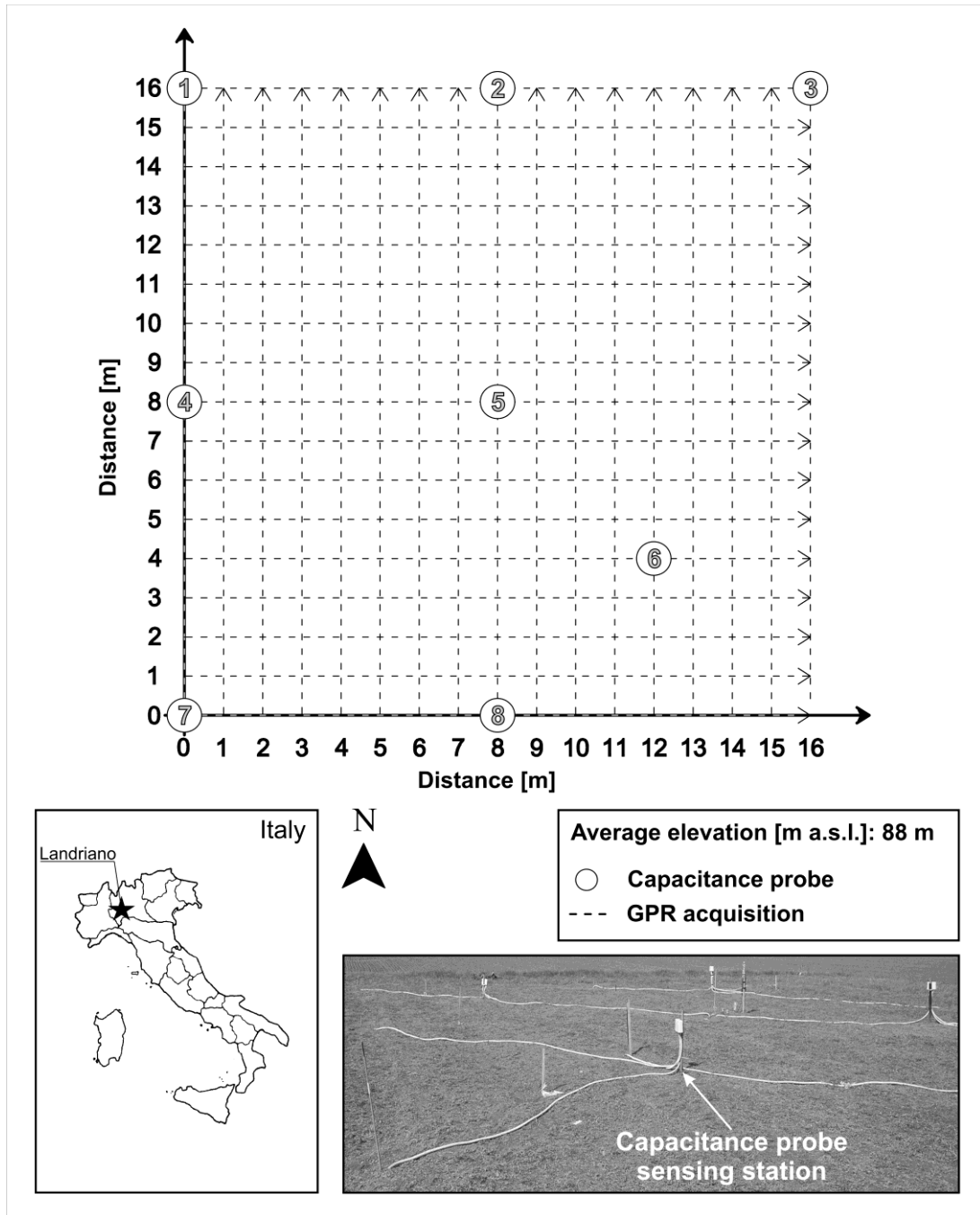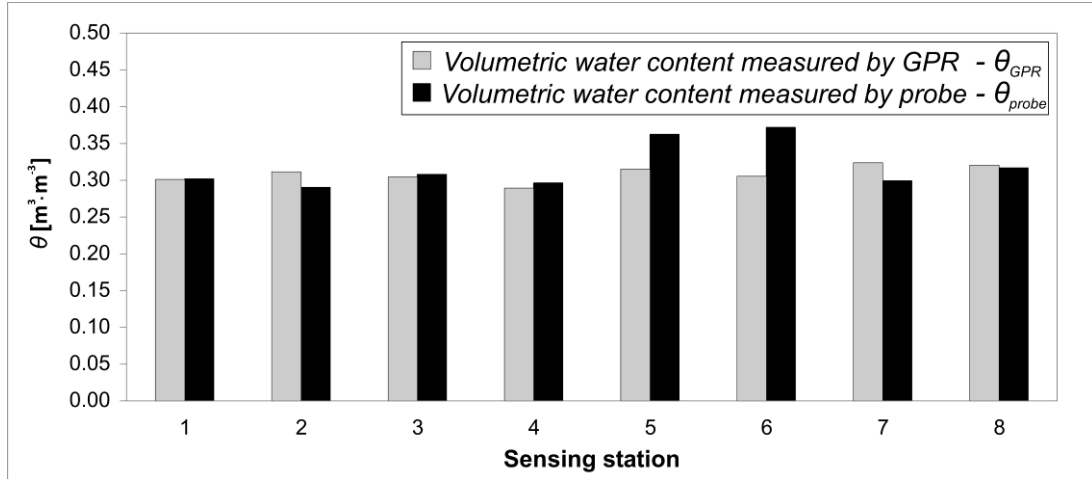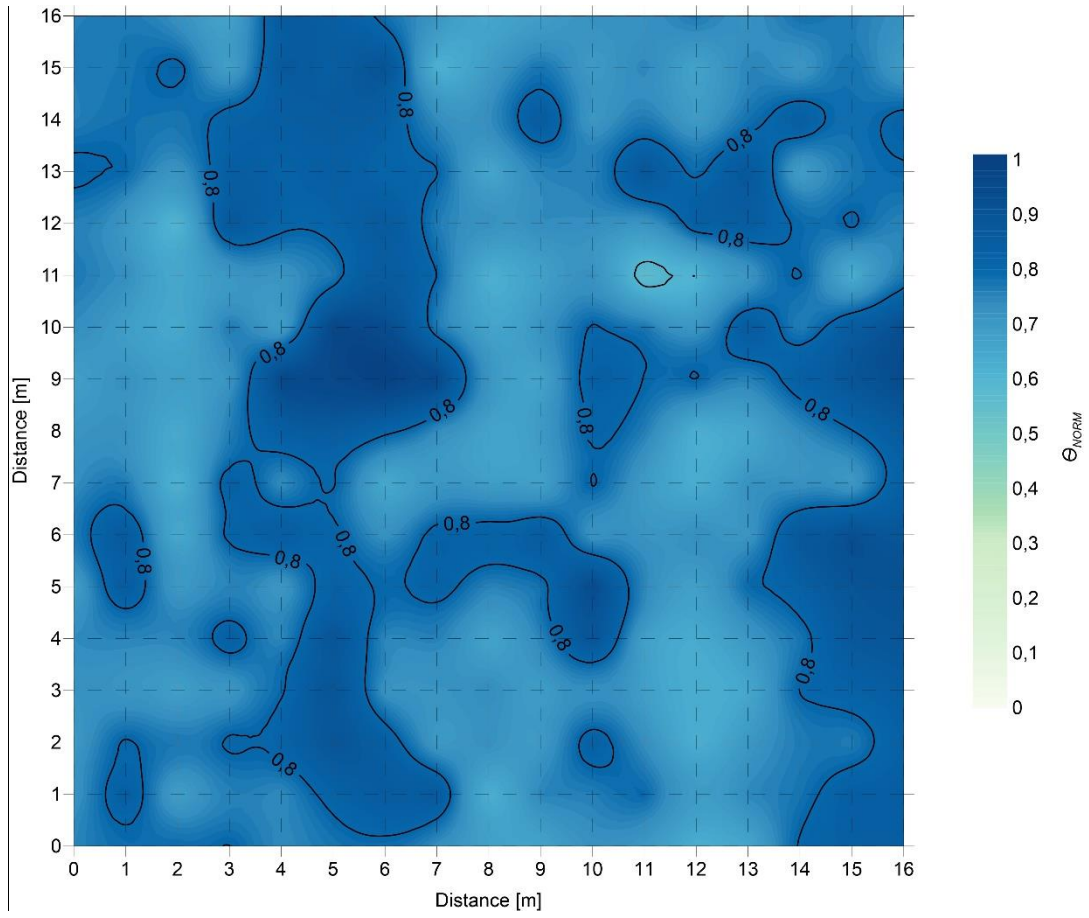FIGURE 1 b) Capacitance probe WaterScout SM100 manufactured by Spectrum Technologies

Inc.

FIGURE 2. Site-specific calibration curve for capacitance probes relating gravimetric (w) and volumetric water content (θ).

FIGURE 3. Study site for the GPR acquisition carried out over a 16m × 16m area, 1m spacing between the tracks (17 × 17 lines square grid pattern).

FIGURE 4. Bar graphs representing GPR-derived (θ_{GPR}) and probe-measured (θ_{probe}) volumetric

soil moisture contents at the eight probe sensing stations.

FIGURE 5. Incidence of moisture residuals at the eight probe sensing stations.

FIGURE 6. a) Normalized shallow soil dielectric moisture (θ_{NORM}) map overlaid with iso-contour lines from the "reflectivity" method.

FIGURE 6. b) Iso-contour lines of the normalized shallow soil dielectric moisture (θ_{NORM}) map from the "reflectivity" method.
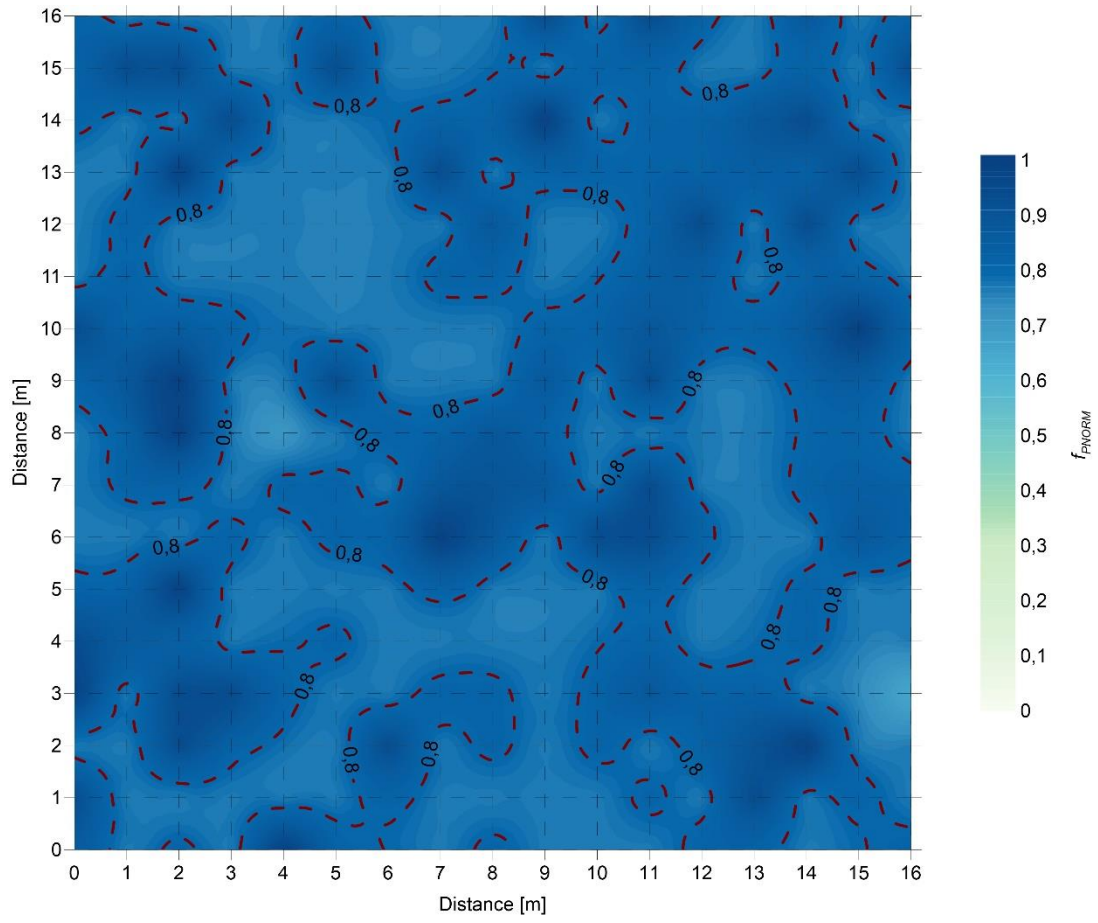
FIGURE 7. a) Normalized frequency peaks (f_{PNORM}) map overlaid with iso-contour lines from the "Rayleigh scattering" method.
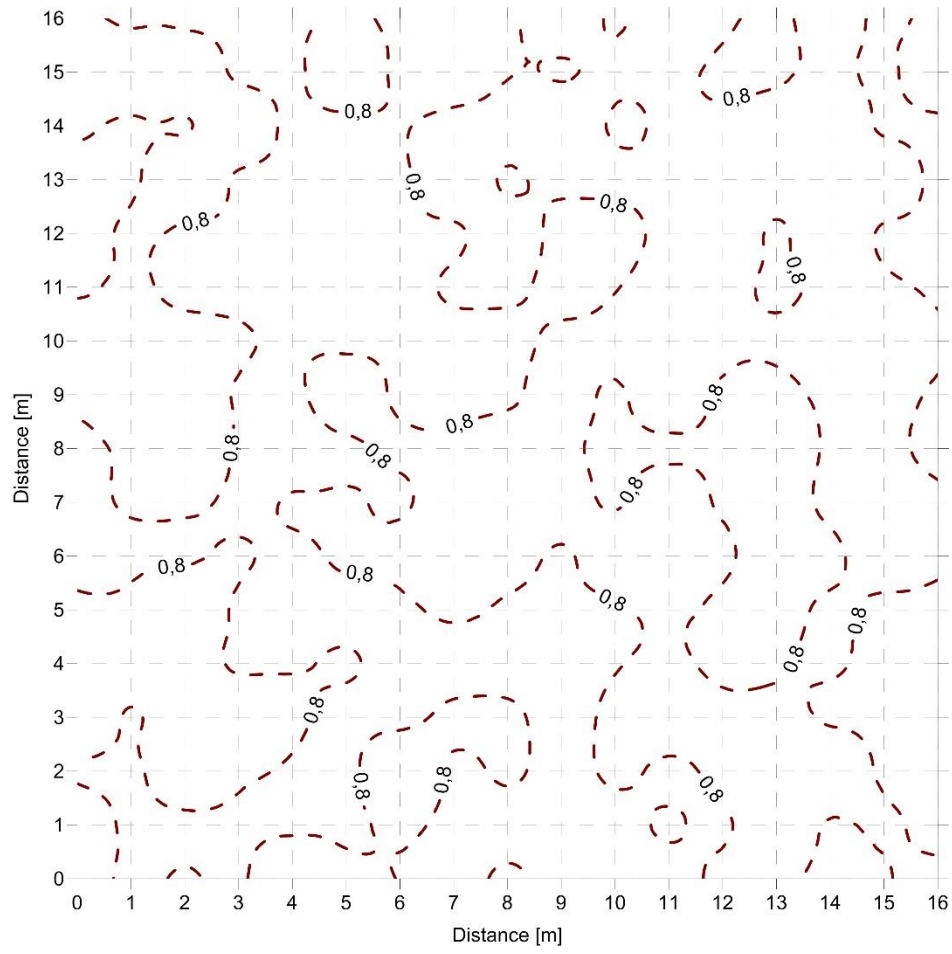
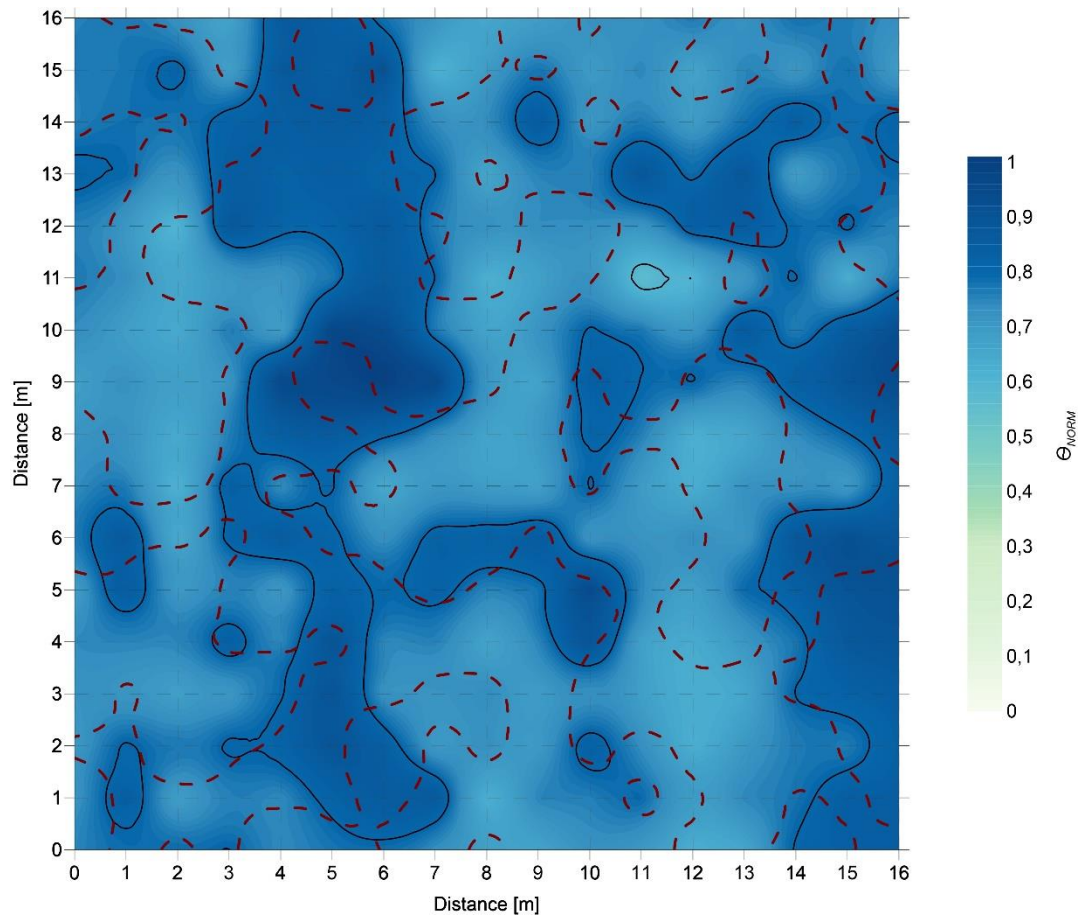FIGURE 7. b) Iso-contour lines of the normalized frequency peaks (*f_PNORM*) from the "Rayleigh scattering" method.

FIGURE 8. a) Normalized shallow soil dielectric moisture (θ_{NORM}) map overlaid with iso-contour lines from the "reflectivity" (solid black lines) and the "Rayleigh scattering" method (dashed red lines).

Tables

TABLE 1. Grain size distribution of a soil sample collected within the test site area.

Sieve [mm]	Grain size			
	$P_{4.75}$	P_2	$P_{0.425}$	$P_{0.075}$
Soil Fraction [%]	99.03	98.51	91.66	53.23